Subcritical Instability and Hysteresis in a Two-Layer Model

SUKYOUNG LEE

Atmospheric and Oceanic Sciences Program, Princeton University, Princeton, New Jersey

ISAAC M. HELD

Geophysical Fluid Dynamics Laboratory/NOAA, Princeton University, Princeton, New Jersey

(Manuscript received 11 June 1990, in final form 7 November 1990)

ABSTRACT

A two-layer quasi-geostrophic model forced by surface friction and radiative relaxation to a jetlike wind profile can exist in either a wave-free state or in a finite-amplitude wave state, over a substantial region of the model's parameter space. The friction on the lower layer must be much stronger than the thermal relaxation, and the upper layer must be nearly inviscid, for this behavior to be observed.

Consistent with this behavior, weakly unstable waves are found that do not stabilize the flow; instead, their growth rate increases with wave amplitude. We attempt to provide a physical explanation for this behavior in terms of 1) the competition between the stabilizing effect of the lower-layer potential vorticity fluxes and the destabilizing effect of nonlinear critical layer formation associated with the upper-layer fluxes, and 2) the tendency of surface drag to restore the vertical shear at the center of the jet by damping the surface westerlies generated by the baroclinic instability.

1. Introduction

The two-layer quasi-geostrophic model has long been recognized as a very useful tool for the study of finite-amplitude baroclinic instability (Phillips 1956; Pedlosky 1970; Williams 1979), but many aspects of its dynamics have yet to be explored. We have examined the statistically steady states of a model that is forced by thermal relaxation to a zonally symmetric "radiative equilibrium" temperature profile in thermal wind balance with a jetlike wind field, and in which the only other dissipative mechanisms are a linear drag on the lower layer wind and scale-selective (biharmonic) diffusion. We focus in particular on the existence in this model of "subcritical instability." For a certain range of model parameters, the radiative equilibrium profile is stable to small disturbances but unstable to large perturbations. As a result the system can exist either in a zonally symmetric state or in a state with O(1) eddy amplitudes. Although results from a two-layer channel model cannot be assumed to be of direct meteorological relevance, they do shed light on the different ways in which baroclinic instabilities can equilibrate. In addition, this result may have implications for the maintenance of storm tracks in the atmosphere.

A similar hysteresis effect is observed in the rotating annulus near the transition between the "upper symmetric" and wave regimes (e.g., Fultz 1959) and has been captured in a truncated spectral model of this system by Lorenz (1962). However, the upper symmetric regime of the annulus owes its existence to the effect of the meridional circulation on the static stability, and this has no analogue in the standard two-layer model with fixed density difference between the layers. At the transition from the lower symmetric to the wave regime, where the dynamics is more analogous to that at the transition to instability in the standard two layer model, no hysteresis of this sort is found in the laboratory experiments or Lorenz's model. Weimer and Haken (1989) describe a weakly nonlinear analysis of a two-layer baroclinic model that exhibits subcritical instability in the very special case in which there are three weakly unstable modes. Steinsaltz (1988) shows that subcritical instability occurs in a two-layer model with a uniformly sloping lower boundary. We do not believe that either of these models is closely related to the results we describe below. Using a model similar to ours, Speranza et al. (1988) present a figure (Fig. 13) which indicates the existence of subcritical instability but do not discuss this fact in their paper.

2. Model description

The dimensionless equations for our quasi-geostrophic two-layer model on a beta-plane are

$$\partial Q_1/\partial t + J(\psi_1, Q_1) = \kappa_T[\{(\psi_1 - \psi_2)/2\} - \tau_e] - \nu\nabla^6\psi_1 \quad (1.a)$$

Corresponding author address: Sukyoung Lee, Geophysical Fluid Dynamics Lab, NOAA, P.O. Box 308, Princeton, NJ 08542.

$$\partial Q_2/\partial t + J(\psi_2, Q_2) = -\kappa_T[\{(\psi_1 - \psi_2)/2\} - \tau_e] - \kappa_M\nabla^2\psi_2 - \nu\nabla^6\psi_2, \quad (1.b)$$

where

$$Q_j = \beta y + \nabla^2\psi_j + (-1)^j(\psi_1 - \psi_2)/2, \quad j = 1, 2. \quad (2)$$

and $j = 1$ and 2 refer to the upper and lower layers respectively. The velocity field is determined by the relation, $(u_j, v_j) = (-\partial\psi_j/\partial y, \partial\psi_j/\partial x)$. The horizontal length scale is the radius of deformation,

$$\lambda = [g(\rho_2 - \rho_1)H/(2\rho_2 f_0^2)]^{1/2}. \quad (3)$$

Here H is the resting depth of either layer. The remainder of the notation is standard. The dimensional (primed) quantities corresponding to those in (2.1) are

$$(\beta', \kappa_T', \kappa_M', \nu') = [\beta U_0/\lambda^2, \kappa_T\lambda/U_0, \kappa_M\lambda/U_0, \nu/(U_0\lambda^3)],$$

where U_0 is the velocity scale. The time is nondimensionalized by λ/U_0.

Ekman damping (κ_M) is included in the lower layer only. The "radiative equilibrium temperature," $\tau_e(y)$, is chosen so as to balance a Gaussian zonal wind shear:

$$U_e = -2\partial\tau_e/\partial y = \exp[-y^2/\sigma^2]. \quad (4)$$

Ignoring the small effect of the biharmonic diffusion, a zonally symmetric solution exists with $U_1 = U_e$ and $U_2 = 0$. Thus, the strength of the upper level wind at the center of the channel in radiative equilibrium can be thought of as setting the velocity scale. We chose $\sigma^2 = 10$ for the calculations in this paper to make the width of the unstable region resemble that in the atmosphere. The channel walls are located at $\pm W/2$. The width W is chosen to be sufficiently large ($W = 21$) that eddy amplitudes are very small near the walls.

The numerical method used to integrate (1) is identical to that in Feldstein and Held (1989), with spectral decomposition in the zonal direction and standard second-order finite differencing meridionally. The biharmonic diffusion terms in (1) represent the enstrophy cascade toward smaller scale, so the value of ν depends on the resolution of the model; as the resolution of the model increases, ν decreases. The extra boundary conditions required by the biharmonic diffusion are also chosen as in Feldstein and Held. A thermal relaxation time scale of 30 days (1 "day" = λ/U_0) is reasonable for the atmosphere, and therefore we hold κ_T fixed at this value unless otherwise stated.

3. Hysteresis and subcritical instability

We first describe results from a model with 16 zonal wavenumbers (0.1 to 1.6), 70 gridpoints between the channel walls, and a biharmonic diffusion coefficient $\nu = 0.006$. The remaining parameters to be varied are β and κ_M. The solid line in Fig. 1 shows the time-averaged eddy kinetic energy

$$\text{EKE} = \int_0^W dy(\bar{u}'^2 + \bar{v}'^2)/2,$$

(where the overbar refers to the zonal mean and a prime to the deviation from the zonal mean), for several values of β, fixing $\kappa_M = 0.2$. The latter value is close to that typically chosen when trying to mimic the atmosphere with a two-layer model. It is more difficult to choose the most meteorologically relevant values of β, since the dependence of baroclinic growth rates on the vertical shear, of which β is a nondimensional measure, is very different in two-layer and continuous atmospheres. These solutions are aperiodic for $\beta \leq 0.25$, and become periodic for $\beta > 0.25$. As described below, all solutions become chaotic as ν is decreased and the meridional resolution increased. The averaging period is 1000 model days. The linear stability boundary, obtained by direct numerical integration of a linearized version of the numerical model, is located at $\beta = 0.27$. For $\beta > 0.27$, the zonally symmetric state is stable, and sufficiently small perturbations decay with time. One might have expected EKE to decrease smoothly to zero at the linear stability boundary, but this is not observed. Solutions with substantial wave amplitude are found up to $\beta \approx 0.36$. These states are obtained by first generating the solution in the linearly unstable region ($\beta < 0.27$) and then slowly increasing β. Thus, there is a range of β for which two states are possible: a stable zonally symmetric state and a periodic state with O(1) eddy amplitude.

The zonal spectrum of the states in the vicinity of the linear stability boundary is dominated by one zonal wavenumber (0.8 for $\beta \geq 0.2$ and 0.7 for $\beta < 0.2$, consistent with the linearly most unstable zonal wavenumbers on the radiative equilibrium flow). One is

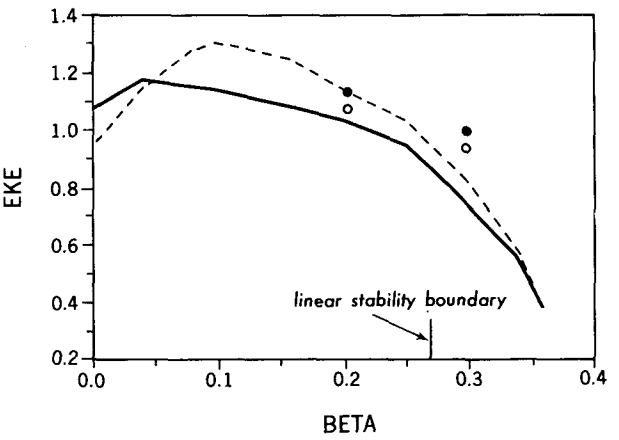

FIG. 1. Time-averaged eddy kinetic energy (EKE) as a function of β. The value of κ_M is fixed at 0.2. Solid and dashed lines are for multiwave and one-wave calculations, respectively, with $\nu = 0.006$. The open dots and filled dots are for multiwave and one-wave calculations, respectively, with $\nu = 0.0001$. The linear stability boundary is also indicated.

therefore tempted to consider a model truncated to retain only one wave and the zonal mean flow. Such a wave–mean flow interaction model is, of course, much more efficient to integrate. The meridional resolution is chosen to be identical to that of the multiwave model, and we choose 0.8 as the single nonzero wavenumber. Use of this one-wave model will be justified a posteriori. The resulting EKE (β) is shown by the dashed line in Fig. 1. In this wave–mean flow interaction model, the wave amplitude is aperiodic for $\beta < 0.10$, periodic for $0.10 \leq \beta < 0.24$, and steady for $\beta \geq 0.24$. Although the transition of the wave state in a one-wave model is different from that in a multiwave model, due to the truncation, hysteresis is once again observed for comparable values of β (the one-wave and multiwave models have the same linear stability boundary), implying that the dynamics underlying this behavior can be studied in this simpler wave–mean flow interaction framework.

If one increases the meridional resolution and decreases the value of the biharmonic diffusion ν, aperiodic solutions evolve from the steady and periodic wave amplitude states. We have performed less diffusive ($\nu = 0.0001$), high resolution (300 gridpoints between the channel walls) multiwave and one-wave model calculations at two points, one in the linearly unstable region and the other in the linearly stable region. The open dots in Fig. 1 are obtained from a model with 20 zonal wavenumbers (0.1 to 2.0) with $\nu = 0.0001$. The filled dots are from the one-wave model. Hysteresis is still present.

One also observes this same phenomenon when κ_M is varied with fixed β. Figure 2 shows EKE as a function of κ_M for $\beta = 0$. The linear stability boundary in this case is located at $\kappa_M = 0.52$ for the one wave-model, and at 0.72 for the multiwave model. (We use $k = 0.8$ once again in the one-wave model. The multiwave model first becomes unstable at $k = 0.7$). Once again,

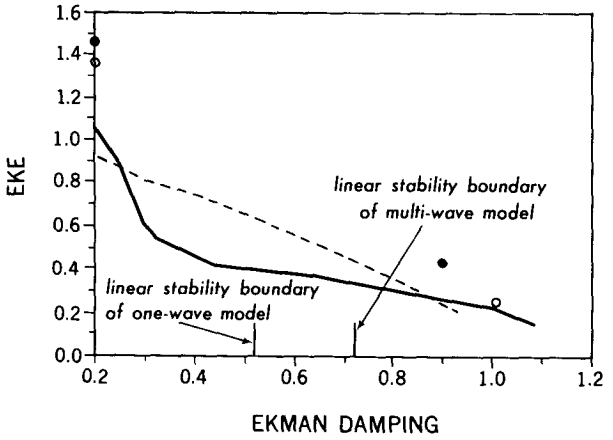

FIG. 2. Same as Fig. 1, except for EKE as a function of κ_M with $\beta = 0$. Note that the linear stability boundaries are different for the one-wave and multi-wave models in this case.

there is a substantial range of κ_M for which a wave-free state and a state with O(1) wave amplitude both exist. As in Fig. 1, we show the results from selected integrations with the high resolution multiwave model, the high-resolution one-wave model, the more diffusive, lower resolution multiwave model, and lower resolution one-wave model. As before, all of the states obtained with the more inviscid models with high meridional resolution are aperiodic, while some of the states of the more diffusive model shown in the figure are steady wave states.

We take advantage of the simplicity of the solutions to the more diffusive model (the steady wave solutions are well resolved with only 70 gridpoints between the channel walls, and one need not integrate for long periods to estimate the time-mean statistics) to explore the parameter space more fully. Using this low resolution one-wave model, we have explored the $\beta - \kappa_M$ plane, with the result shown in Fig. 3a. The linear stability boundary is denoted by the dotted line. The thick solid line marks the hysteresis boundary, beyond which the wave-free state is the only one found in our time integrations. The contours in this plot represent the eddy kinetic energy. The dashed line in the figure marks the transition from steady to vacillating wave amplitudes. We do not study this transition in detail, since we know that it is sensitive to the diffusion; the region of steady states contracts as the meridional resolution increases and ν decreases until it disappears entirely.

The sheet of solutions that results in the hysteresis illustrated above emerges from the other sheet near $\kappa_M = 0.06$, $\beta = 0.337$. There is a small region near this point in which two distinct states with nonzero wave amplitude exist.[1] Figure 3b shows this region in more detail, in a three dimensional perspective. As in Fig. 3a, the linear stability boundary is indicated by the dotted line. The thick solid and dashed lines indicate the boundary of the upper sheet and the lower sheet of solutions, respectively. The projection of the boundaries of the upper and lower sheet of solutions onto the zero-EKE surface are denoted by the dashed-dotted lines: the curve $\widehat{x'y'}$ is the projection of the curve $\widehat{xy}$ onto the zero-EKE surface; similarly $\widehat{y'z}$ is a projection of $\widehat{yz}$ onto this surface. We presume that there are also unstable solutions which connect the upper and the lower sheet of solutions.

Figure 4 shows the zonal mean flow and potential vorticity gradients in the one-wave model at point A, which is in the linearly stable region in Fig. 3a ($\kappa_M = 0.2$, $\beta = 0.30$). The low-level flow has been accelerated near the center of the channel, while there is strong deceleration in the upper layer on the jet margins. The phase speed of the steady wave is 0.174, so this deceleration is located close to the wave's critical latitudes. At the center of the channel, the upper layer

[1] See *Note added in proof.*

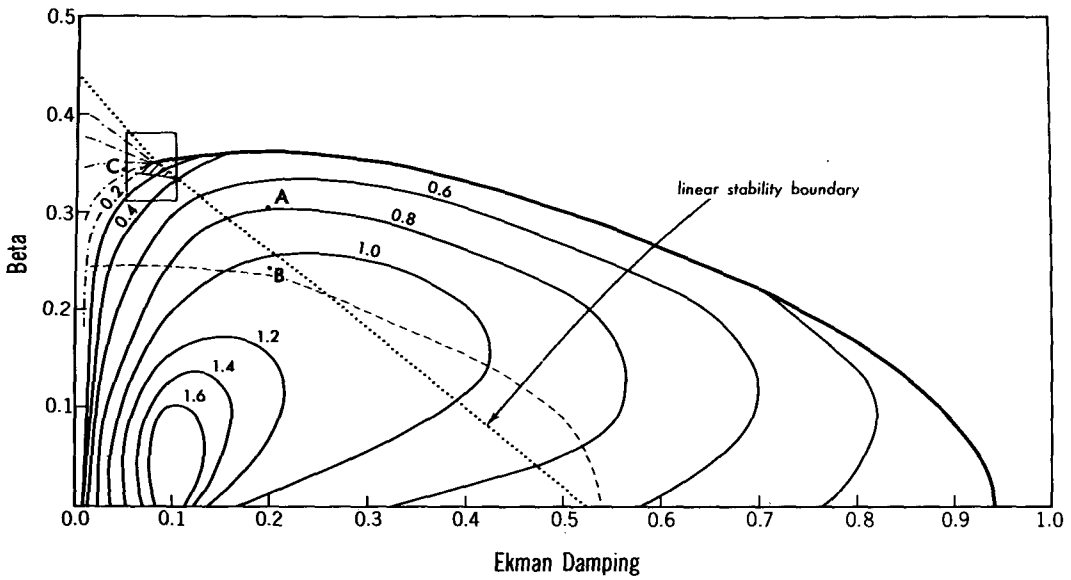

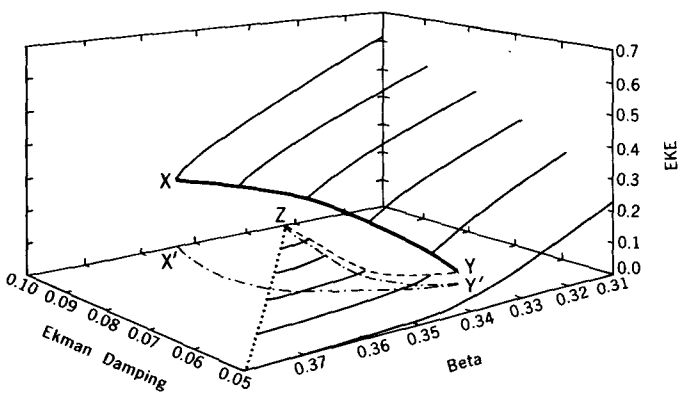

FIG. 3. (a) The contour plot of EKE in $\beta - \kappa_M$ plane, obtained from one-wave model calculations (for $\nu = 0.006$). The contour interval is 0.2. The dashed–dotted lines in the upper-left corner of the figure are contours for small values of EKE; the values of the contours are 0.005, 0.01, 0.02, 0.04, and 0.08, starting from the contour near the linear stability boundary. The thick solid line marks the hysteresis boundary, beyond which the wave-free state is the only solution. The dashed line marks the transition from steady to vacillating wave amplitudes. (b) A three-dimensional perspective of the solutions focused on a region (the box indicated in Fig. 3a) where two distinct states with non-zero wave amplitude exist (shaded area in Fig. 3a). See text for more description.

wind is accelerated, and the vertical shear actually increases slightly. The potential vorticity gradient in the upper layer has been reduced sharply near the critical latitude on the jet margin (see Fig. 4b). The structure of the time-averaged zonal mean flow remains quite similar as the number of zonal waves is increased and the diffusivity in the model is decreased (not shown). Nonlinear critical layer dynamics evidently is at least partly responsible for the unsteadiness found in the higher resolution models.

The system is clearly very inefficient at reducing the vertical shear in the region where the shear is initially the largest, but the shear is reduced to the north and south of the jet where the critical latitudes exist. By stabilizing the regions on each side of the jet, without stabilizing the flow near the jet center, the eddies have contributed to their own meridional confinement.

When the low resolution, diffusive wave–mean flow interaction model evolves into a state with a steady wave superposed on a steady zonal flow, the wave satisfies the linear equation for normal mode disturbances on that flow. It follows that the modified zonal flow must support a neutral mode with the structure of the steady wave. All the normal modes of the unmodified flow at point A are damped. In this sense, the wave has decreased the stability of the zonal flow.

To illustrate this point further, we examine the initial evolution of a very small disturbance to the radiative equilibrium flow at the points B and C in Fig. 3a. The point B (C) is chosen to represent a weakly nonlinear state near the stability boundary at which hysteresis is (not) observed. The low resolution diffusive one-wave model is used for this purpose. Forcing and dissipation are retained as in the full model. The flow is weakly unstable at both points. The initial condition is of sufficiently small amplitude that the normal mode structure is achieved before the solution becomes nonlinear. Figure 5 shows the instantaneous growth rate, defined as $\partial_t \ln(\mathrm{EKE})$. At point C, the growth rate decreases with time; at point B it increases in time, in which case

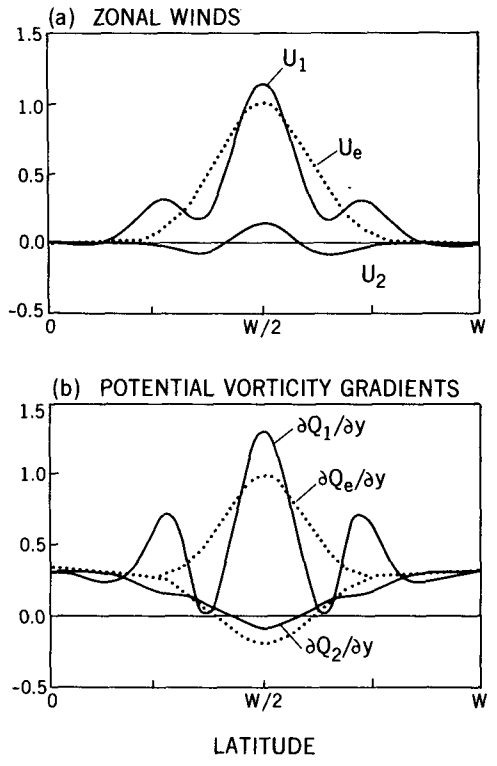

FIG. 4. (a) Time-averaged zonal mean winds and (b) time-averaged zonal mean potential vorticity gradients from the one-wave calculations (with $\nu = 0.006$) for $\beta = 0.3$ and $\kappa_M = 0.2$. The dotted line is the "radiative equilibrium" state.

the wave cannot be expected to equilibrate at a small amplitude, consistent with Fig. 3a.

Formally, the wave amplitude evolution equation is expected to be of the form (see Pedlosky 1970 or Weimer and Haken 1989) $\partial_t A = \alpha A + \gamma |A|^2 A$ for small A. Evidently Re(γ) changes sign between B and C. If we move the point B to the other side of the linear stability boundary, Re(α) will become negative but Re(γ) will still be positive, and subcritical instability will exist. While one could try to compute γ using weakly nonlinear theory, it is not clear that such an analysis would shed any light on why the mean flow modification due to a weakly unstable mode should tend to destabilize the flow further. While we are not satisfied that we have a complete physical explanation for this result we strongly suspect that it is related to the mean flow modification near the upper layer critical latitudes, particularly to the sharp reduction in the potential vorticity gradient, and to the tendency of the surface friction to regenerate the vertical shear at the center of the jet.

A small amplitude disturbance incident on a critical latitude is absorbed, at least partially, if $\partial_y Q_j > 0$. As the gradient is reduced, the absorption decreases. Perfect reflection, with no absorption, occurs if the gradient vanishes at the critical latitude. By reducing the gradient near the critical latitudes in the upper layer, the disturbance is therefore eliminating a sink of wave activity. The wave has created for itself a "channel" between the poorly absorbing nonlinear critical layers within which it is more easily sustained by baroclinic instability (see Fig. 4b).

One is led to think in terms of a competition, as the wave grows, between the stabilization due to the reduction of the negative potential vorticity gradient in the lower layer and the destabilization due to this critical layer effect in the upper layer. This picture helps explain why the destabilizing effect should become dominant as the surface damping is increased, as in Figs. 3a and 3b; the eddies have more difficulty in modifying the lower-layer potential vorticity gradient when the lower-layer winds are strongly damped, while the destabilizing upper-layer fluxes are relatively unaffected by the friction. This dynamics is qualitatively similar to that in the barotropic initial value problem of Hou and Farrell (1985), in which a stable zonal flow is modified by a finite-amplitude wave in such a way that it can then maintain the wave.

The friction on the zonal mean flow in the lower layer also has an effect on the subcritical instability. When the forcing and dissipation are arbitrarily removed from the zonal mean equations, growth rates are found to decrease with time at B as well as at C, and there is no longer a subcritical instability near B. However, if one moves to the right along the linear stability boundary in Fig. 3a (toward larger κ_M and smaller β), and repeats the initial value calculation, one again finds a point at which growth rates increase with time. By damping the low-level zonal mean westerlies generated by the baroclinic instability, the surface drag tends to restore the vertical shear at the center of the jet, making it harder for the wave to stabilize the flow, thereby enhancing the subcritical instability. The effect of the low-level zonal mean drag cannot in itself account for the hysteresis in the model; it cannot explain why the mean flow as modified by the instability

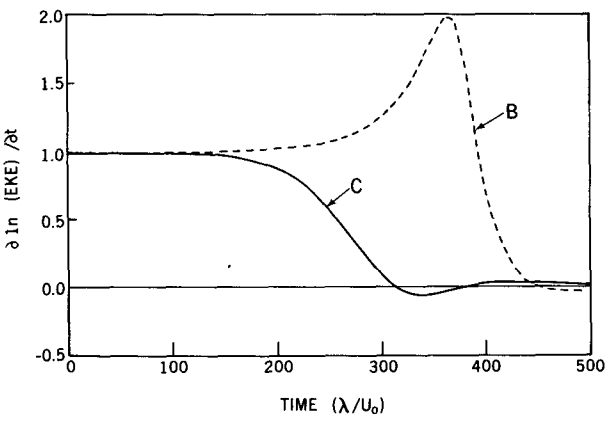

FIG. 5. The instantaneous growth rate; $\partial_t \ln(\text{EKE})$. The solid and dashed lines correspond to points C and B in Fig. 3a, respectively. The growth rate is nondimensionalized by its initial value.

(as in Fig. 4) can support a linear neutral mode, while the unmodified mean flow possesses damped normal modes only. Both the "critical layer" character of the mean flow modification of the upper layer and the tendency of the surface drag to sustain the vertical shear appear to be needed to explain the model's behavior.

The low resolution, diffusive multiwave model possesses a very similar subcritical instability. The growth of the most-unstable zonal wavenumbers begins to increase before other zonal waves begin to grow substantially, helping to justify the qualitative use of the one-wave model to study the subcritical instability.

When the meridional resolution in the one-wave model is increased and the diffusivity lowered to the point that the final state is aperiodic rather than steady, the initial-value problem for a small disturbance exhibits more complex behavior that we have not fully analyzed.

We have examined the qualitative behavior of the one-wave model when linear Ekman damping is included in the upper as well as the lower layer. For this purpose, we set $\beta = 0$, since the range of Ekman damping where one can observe hysteresis is relatively large when $\beta = 0$ (see Fig. 3a). In these experiments the mean flow is forced in such a way that ($U_1 = U_e$; $U_2 = 0$) is the solution in the absence of eddies (ignoring the biharmonic diffusion); in particular, the upper layer friction is assumed to relax the upper layer flow to $U_e(y)$. This kind of forcing is not relevant to the troposphere, but we utilize it here because it is simpler to compare models in which the eddy-free mean flows are identical. When the two Ekman damping rates and the thermal damping rate are all equal (producing a linear damping on the potential vorticity), no hysteresis between wave-free and wavy states is observed. When the thermal damping is held fixed at 1/30, no hysteresis is observed once the ratio (ϵ) of the upper layer to the lower layer Ekman damping exceeds ≈ 0.1. Figure 6 shows the time-averaged EKE for several values of ϵ with varying lower-layer Ekman damping (κ_M). Once again we use the one-wave, low resolution model with $k = 0.8$. In the same figure, linear stability boundaries are also indicated for each ϵ. The region of hysteresis shrinks as ϵ increases, and finally disappears when ϵ exceeds 0.1. This result is consistent with the dynamics outlined above, in that the upper layer flow must be relatively free to respond to the eddy stresses for the hysteresis to be present; this requires that both the thermal damping and the upper layer momentum damping be small compared to the momentum damping in the lower layer.

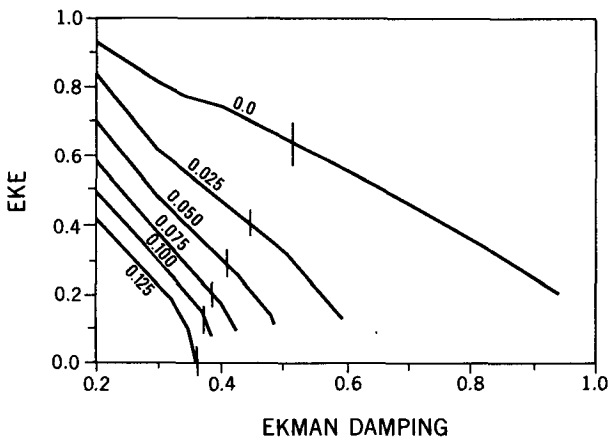

FIG. 6. Time-averaged eddy kinetic energy (EKE) as a function of κ_M for several values of ϵ (see text for definition). The numbers along the lines are the corresponding values of ϵ. The location of the linear stability boundary for each ϵ is indicated by a vertical line on each curve.

4. Concluding remarks

In a two-layer model for which the mechanical damping is much weaker in the upper than in the lower layer, and in which the "radiative equilibrium" state is jetlike, hysteresis can occur between wave-free states and states with O(1) eddy energy. One cannot expect this hysteresis to be directly relevant to the atmosphere. Even if one accepts the fact that the observed zonal mean flow may not be far from being stabilized by strong surface friction (see Farrel 1985; Lin and Pierrehumbert 1988), the state that the atmosphere would reach in the absence of eddies would certainly be very far from stability, not only because of larger horizontal temperature gradients but, even more so, because of a much smaller static stability. It is not so much our choice of parameters in the two-layer model that prevents the direct meteorological relevance of this result, but the unphysical way in which the static stability is prescribed in this quasi-geostrophic model.

Yet, these results still raise interesting questions concerning more realistic atmospheric models and the different ways in which baroclinic instabilities can equilibrate. Our attempt at explaining the behavior of the two-layer model involves a competition between the stabilizing effect of low-level potential vorticity fluxes and the destabilizing effect of nonlinear critical layer formation associated with upper level fluxes. The latter is "destabilizing" in that it prevents the eddy from decaying barotropically through meridional dispersion. This may be a common feature in the nonlinear evolution of baroclinic instability on jets. Also playing a role in the subcritical instability is the tendency of surface drag to restore the vertical shear at the center of the jet, by damping the surface westerlies generated by the instability. Combined with the fact that the deceleration of the upper layer flow takes place primarily to the north and south, but not at the center of the jet, the result is that the system is very inefficient at reducing the vertical shear in the region where this shear is initially the largest. Such behavior may be relevant to the maintenance of storm tracks in the atmosphere.

Note added in proof. Some of the details in Fig. 3 have been found to be sensitive to the diffusivity in the model. When ν is lowered to 0.0001 in the one-wave model, and the meridional resolution increased, the region where there are two solutions with nonzero EKE expands somewhat. The lower sheet of solutions is found to exist in a very narrow region adjacent to the linear stability boundary for values of κ_M as large as 0.35. This region is so narrow that only the upper sheet of solutions exists at point B in Fig. 3a, but as one moves even closer to the linear stability boundary, the small amplitude state eventually appears. It may be that in the limit of infinitesimal diffusivity and infinite resolution, the small amplitude state exists for all κ_M, in an extremely narrow region close to the linear stability boundary. The hysteresis boundary also expands slightly as the diffusivity is lowered. The basic structure shown in Fig.3a remains unchanged.

Acknowledgments. One of the authors (SL) was supported by National Science Foundation Grant ATM 8800667.

REFERENCES

Farrell, B., 1985: Transient growth of damped baroclinic waves. *J. Atmos. Sci.*, **42,** 2718–2727.

Feldstein, S. B., and I. M. Held, 1989: Barotropic decay of baroclinic waves in a two-layer beta-plane model. *J. Atmos. Sci.*, **46,** 3416–3430.

Fultz, D., R. R. Long, G. V. Owens, W. Bohan, R. Kaylor and J. Weil, 1959: Studies of thermal convection in a rotating cylinder with some implications for large-scale atmospheric motions. *Meteor. Monogr.*, Vol. 4, No. 21, Amer. Meteor. Soc., 104 pp.

Hou, A. Y., and B. Farrell, 1986: Excitation of nearly steady finite-amplitude barotropic waves. *J. Atmos. Sci.*, **43,** 720–728.

Lin, S.-J., and R. T. Pierrehumbert, 1988: Does Ekman friction suppress baroclinic instability? *J. Atmos. Sci.*, **45,** 2920–2933.

Lorenz, E. N., 1962: Simplified dynamics equations applied to the rotating-basin experiments. *J. Atmos. Sci.*, **19,** 39–51.

Phillips, N. A., 1956: The general circulation of the atmosphere; a numerical experiment. *Quart. J. Roy. Meteor. Soc.*, **82,** 123–164.

Pedlosky, J., 1970: Finite amplitude baroclinic waves. *J. Atmos. Sci.*, **27,** 15–30.

Speranza, A., and P. Malguzzi, 1988: The statistical properties of a zonal jet in a baroclinic atmosphere: a semilinear approach. Part I: Quasi-geostrophic, two-layer model atmosphere. *J. Atmos. Sci.*, **45,** 3046–3061.

Steinsaltz, D., 1988: Instability of baroclinic waves with bottom slope. *J. Phys. Oceanogr.*, **17,** 2343–2350.

Weimer, W., and H. Haken, 1989: Chaotic behavior and subcritical formation of flow patterns of baroclinic waves for finite dissipation. *J. Atmos. Sci.*, **46,** 1207–1218.

Williams, G. P., 1979: Planetary circulations: 3. The terrestrial quasi-geostrophic regime. *J. Atmos. Sci.*, **36,** 1409–1435.